Original Articles

Integration of historical map and aerial imagery to characterize long-term land-use change and landscape dynamics: An object-based analysis via Random Forests

Dan Liu[a], Elizabeth Toman[a], Zane Fuller[a], Gang Chen[b], Alexis Londo[a], Xuesong Zhang[c,d], Kaiguang Zhao[a,e,*]

[a] School of Environment and Natural Resources, Environmental Science Graduate Program, The Ohio State University, Columbus, OH 43210, USA
[b] Laboratory for Remote Sensing and Environmental Change, Department of Geography and Earth Sciences, University of North Carolina at Charlotte, Charlotte, NC 28223, USA
[c] Joint Global Change Research Institute, Pacific Northwest National Laboratory/University of Maryland, College Park, MD 20740, USA
[d] Earth System Sciences Interdisciplinary Center, University of Maryland, College Park, MD 20740, USA
[e] Ohio Agricultural Research and Development Center, School of Environment and Natural Resources, The Ohio State University, Wooster, OH 44691, USA

ARTICLE INFO

ABSTRACT

Tracking Earth's past helps us to move from hindsight to foresight in seeking landscape sustainability, a pursuit aided by modern mapping capabilities but hindered by a dearth of historical landscape information. To fill the data gap and exemplify the use of old maps for land-use change sciences, we combined an old paper-based US civil war map and modern aerial photos to derive land-use history and landscape dynamics at fine scales for a region near Chancellorsville, USA, from 1867 to 2014. We also tested how advanced algorithms—object-based image analysis and Random Forests (RF)—could aid in data processing. Automatic classification of the scanned 1867 paper map proved difficult, but its manual digitization could benefit from object-based image segmentation. Classifying digital aerial images was more accurate via the object-based than pixel-based method, but only if the images were segmented appropriately. In the object-based classification, spectral-based features were much more important and useful than shape/geometry features for land-cover discrimination, as ranked by RF. During the 147 years, 32% of the region changed in land type. Settlement and roads increased in extent by 1850% and 691%, respectively, and woodland decreased by 19%. These changes fragmented the landscape, altered the hydrological regime, and affected river morphology. The utility of old maps exemplified here provides an impetus for leveraging extant old maps or historical records to support land-use and global change research. Our study also connotes the importance of preserving and geotagging current non-traditional data, such as photos, videos, and citizen science data, that can serve as a baseline to document future landscape change.

1. Introduction

The pace of contemporary global environmental change is unprecedented, driven largely by humans. Of the myriads of ways we affect Earth, land alteration stands out (Foley et al., 2005). Land-use activities often clear natural vegetation, disturb carbon pools, impair biodiversity, modify hydrology, and impact climate, among others (Bright et al., 2017; Lambin and Geist, 2008; Mahowald et al., 2017). Understanding the patterns, drivers, and impacts of landscape change, therefore, is essential to seeking solutions for landscape sustainability (Wu, 2013). Central to these pursuits are observations and technologies capable of accurately tracking where, when, and how lands have changed (Olah, 2009; Zhao et al., 2018).

Nowadays, monitoring land status is dominated by the use of spatial imaging technologies (Joshi et al., 2016). The wealth of remotely-sensed imagery captures vagaries of Earth's dynamic landscapes across spatial scales, be it a treefall, a new plantation, a wildfire, a removed dam, or an expanding city (Arnett et al., 2015; Chen et al., 2015; Gitas et al., 2014; Shalaby and Tateishi, 2007; Xiao et al., 2006; Zhou et al., 2015). Their use is helping glean insights into land-use change

---

processes, such as the underlying socioeconomic drivers and associated climatic impacts, and inform sound decisions (Mahowald et al., 2017; Newbold et al., 2015; Zhao and Jackson, 2014). Such mapping capabilities continue to advance, enabling us to routinely observe areas as large as the globe and as fine as a tree or even finer (Congalton et al., 2014; Pu and Landry, 2012; Zhao et al., 2015). The recent opening of Landsat archives, for example, allows mapping forest loss and gain for each 30-m land pixel of the globe (Hansen et al., 2013); even more, such information can be put at our fingertips instantly through webGIS portals or digital earth platforms (e.g., Google Earth).

Accompanying the rapid growth of geospatial data is steady improvement in data analytics. For example, the set of algorithms for classifying land-cover and vegetation type has been expanding, including many machine learning tools such as Random Forests, Gaussian Processes, and Support Vector Machine (Belgiu and Drăguţ, 2016; Li et al., 2016; Zhao et al., 2011). The past two decades also saw a rise in the use of high-resolution imagery that can resolve individual spatial entities, fostering a new analysis paradigm known as object-based image analysis (OBIA) (Chen et al., 2012; Walter, 2004). Its essence is to group neighboring pixels into objects, a process aided by the development and availability of image segmentation algorithms. OBIA is not just conceptually appealing but practically powerful. Experimental evidence is accumulating to exemplify its advantages over pixel-based image classification, especially when analyzing high-resolution images with limited spectral information (e.g., three or four bands) and for heterogeneous landscapes (Blaschke, 2010). The recent surge in OBIA is attributed largely to the growing availability of software. The majority of published studies, for example, rely on eCognition, a mainstream commercial OBIA software system (Blaschke, 2010). Meanwhile, the use of OBIA still faces some practical challenges, as highlighted in a recent review by Hussain et al. (2013). Examples of questions to be further explored include how to find the optimal segmentation parameter for a given scene, how to address change detection at object levels when confronted with some inevitable sources of error, and how to leverage machine learning techniques to further improve OBIA.

Despite the well-established capabilities for mapping current land status, there is a scarcity of historical land-use/land cover data (Prestele et al., 2017). Modern remote sensing began long after World War II (Jensen, 2009). Maps of landscape composition prior to that are rare or nonexistent for large parts of the world, but historical landscape data have critical roles to play. They document past human impacts and provide clues on tackling current environmental issues, such as urban planning, food security, land policy, and climate mitigation (Lambin and Geist, 2008): A lack of data of the past makes it hard to build predictive understandings for the future. We can't observe Earth retrospectively, so all extant data can be valuable for inferring the past landscape. Goldewijk (2001) translated historical population density into global cropland distributions for the past 300 years. In the US, paper records of witness trees helped to reconstruct pre-settlement vegetation pattern (Srinath and Millington, 2016). Relicts such as stonewalls under forests aid in delimiting long-abandoned agriculture fields (Johnson and Ouimet, 2016). Other examples include the use of deeds and sale records, tax valuation, travelogue, ancient script, diary, letter, folklore, drawings, and old maps (Killeen et al., 2008; Orwig and Abrams, 1994; Ostafin et al., 2017).

Of all extant historical sources describing landscapes, old maps are of particular importance. Historical drawings or paper maps, such as topographic, cadastral, and military maps, are the only data sources that capture the past landscapes of a region in a true spatially-explicit manner. These maps sometimes are dated back several centuries and are valuable for studying long-term land-use history and vegetation dynamics. Their utility is growingly recognized; community interest in mining old maps is rising (Bičík et al., 2015). As examples, Cousins (2001) combined non-geometric historical maps with aerial photos to analyze land use/land cover change in south-east Sweden. Haase et al. (2007) analyzed multiple old topographic maps for Saxony, Germany to track landscape changes and tackle contemporary environmental issues. Fuchs (2015) incorporated historic statistics and old topographic maps into reconstructions of land cover/land use for Central Europe back to 1900.

Use of old maps to fill data gaps not just brings prospects to land change research but also presents some practical challenges. Foremost, old maps are diverse in nature and are incompatible with modern digital maps in terms of map projection, survey methods, spatial details and scales, and thematic representation (Foster, 1992; Loran et al., 2017; Petit and Lambin, 2002a; Schaffer and Levin, 2016). Most early maps are non-geometric (Cousins, 2001). Map distortion is difficult to quantify and rectify, even with many ground control points. The geometric correction may be invalid for local features, which is of no concern for coarse-level analyses but problematic for fine-scale analyses. Further, unlike remote sensing imagery that records true physical signals, old maps are secondary—sometimes, subjective—representations of spatial objects. Their interpretation needs expertise, caution, and even educated guesses. This is particularly true if metadata are lacking or information desired is rendered only implicitly in the old maps. Currently, old maps are predominantly analyzed manually (Pavelková et al., 2016). Uncertainties exist regarding how modern image analysis techniques can facilitate the information extraction from old maps. Overall, large gaps still remain in research on the integrated use of old paper maps and modern digital imagery for landscape change analysis, urging for more cases studies, especially those focusing on fine-scale landscape characterization.

This study aims to exemplify the use and value of historical map in characterizing land-use history and landscape dynamics. We conducted a case study for a region near Chancellorsville, Virginia, USA, through the combined use of an 1867 civil war map and modern aerial images. Our purpose is three-folded. First, we attempted to determine the extent to which the modern image analysis technique—object-based analysis—can improve the processing of historical map. We also examined the use of machine learning—Random Forests—in aiding in object-based classification of digital aerial images. Second, we provided fine-scale characterization and maps of land-use history from 1867 to 2014 for the region, a product not previously available for this historically important landscape. Third, we sought to demonstrate the implications of the new land change maps by explaining the patterns or drivers of the landscape dynamics and quantifying the associated consequences in terms of changes in landscape metrics as well as in river morphology.

2. Materials and methods

2.1. Study area

Our study area is a 110 km^2 region near Chancellorsville, Virginia, a place known for the Battle of Chancellorsville in 1863 (Fig. 1). Large part of it falls within Spotsylvania County, which was established in 1721. The region straddles the Piedmont Plateau and Coastal Plain physiographic provinces, with characteristic soils being strongly acidic and low in fertility. Vegetation prior to 1721 (i.e., pre-European settlement) was mixtures of deciduous forests and was believed to be disturbed by Indians to some degree through frequent burning of woodlands (Mansfield, 1977). This fire regime had favored fire-resistant oaks, leading to a climax landscape of oak-hickory forests. European settlement transformed the landscape dramatically (Orwig and Abrams, 1994). Large fractions of the forests were cleared for firewood to support iron production or for agriculture lands to produce tobacco and cotton. Poor cultivation practices soon led to severe soil erosion and eventually to agriculture abandonment. Much of the cleared lands then became recovered to forests. The modern landscape of the region has also seen rapid changes during the past few decades, attributed in part to the rise in population.
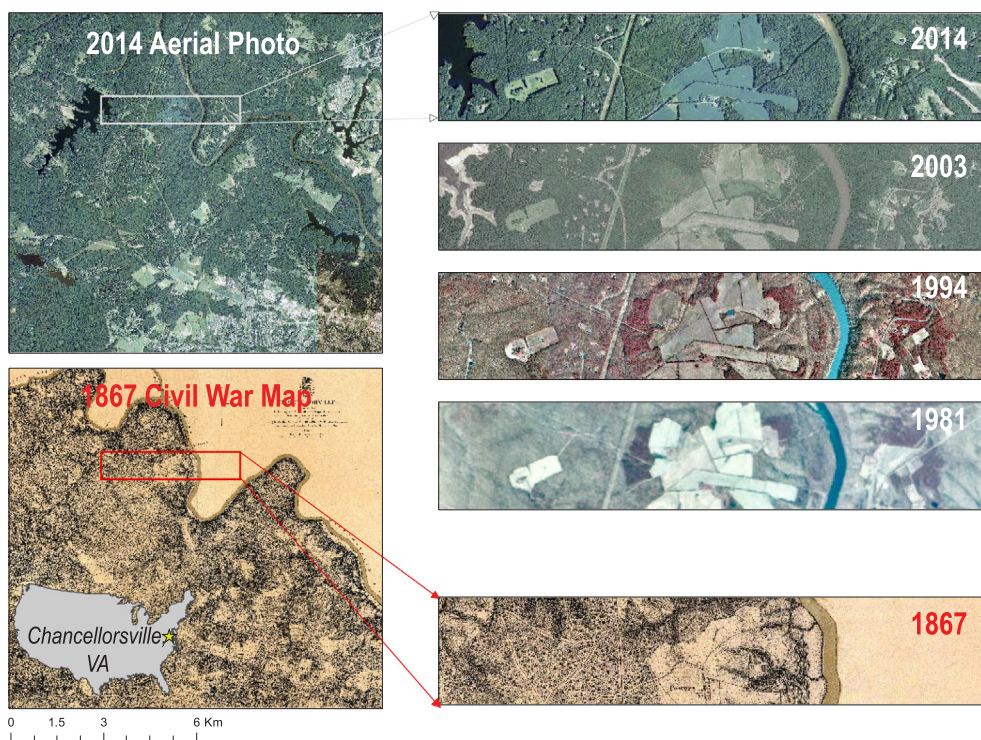
Fig. 1. Study area (left) and data used: A paper-based 1867 US civil war map and four modern aerial photos (right).

2.2. Old map and aerial imagery

To characterize long-term spatially-explicit land use changes over our study area at fine resolutions, we complied a paper-based historical map and multiple aerial photos from several sources (Table 1), spanning from 1867 to 2014. Specifically, the old paper map used is a civil war map made in 1867 by Cartographer Nathaniel Michler under the authority of the U.S. War Department. It is among the most accurate battlefield maps of that time, depicting details about houses, fences, names of residents, roads, vegetation, drainage, rivers, and fords in Northern Spotsylvania (Fig. 1). On the map, relief was marked by hachures—some strokes drawn in the direction of the steepest slope to represent terrain. We obtained a scanned version of it from David Rumsey's Historical Map Collection. The paper version has a scale of 1:21,120 and the digital photocopy has 300 pixels per inch, giving an apparent pixel size of 1.77 m. The photocopy has three bands (i.e., RGB) with a yellow background and rivers colored in green, but inherently, the map is a single-band image because its key map features were drawn in monocolor.

The aerial photos were obtained from USGS' and USDA's geospatial gateways for four points in time across 35 years: 1981, 1994, 2003, and 2014 (Fig. 1). All the photos are three- or four-band natural color/color-infrared images, roughly with a 1-m spatial resolution. The images were collected in different national aerial photography campaigns (Table 1). The 1981 imagery is film-based and photoscanned: It is not georeferenced. In contrast, the images for the three later years were collected

with digital cameras and have been accurately georeferenced. Satellite multispectral images captured between 1981 and 2014 are available from many sources or platforms, such as Landsat (as early as 1972), SPOT, and Quickbird. Pre-1981 photographic images also exist from several sources, such as the US declassified CORONA imagery (available as early as 1962), the USGS aerial single frame atlas, and the aerial photography collection from the US national archives and records administration. These additional data can improve the temporal resolution of our analysis to a certain degree, but we made no attempt to compile the extra potential data, due to various constraints that include, but are not limited to, coarser image resolutions, data costs, restrictive access, partial coverage, and unconventional processing. Interpreted differently, our primary goal here is to obtain at least one modern aerial photo to contrast with the 1867 map rather than search for all available data to generate a continuous record of land cover with a minimal time gap.

2.3. Data analysis and image classification

Not all the data compiled above are georeferenced. Our data processing therefore started with georectifying the 1867 old map and the 1981 aerial image. In the georeferencing, the 2014 aerial photo was chosen as the baseline and we manually selected ground control points. Georefencing the 1981 aerial photo was straightforward, but the 1867 old map needed extra care and sometimes trial-and-error, due to both its different nature and the dramatic landscape change over the

Table 1
Description of data sources and characteristics.

Data	Year of acquisition	Color	Resolution (M)	Source
Paper-based Civil war Map	1867	Monocolor	1:21,120	D. Rumsey's Map Collection
National High Altitude Photography (NHAP)	1981	color-infrared	1:58,000	USGS
Digital Orthophoto Quadrangle (DOQs)	1994	color-infrared	1	USGS
National Agriculture Imagery Program (NAIP)	2003	natural color	1	USDA
National Agriculture Imagery Program (NAIP)	2014	natural color	1	USDA

Table 2
Classification schemes for land-use change analysis.

Classification	Description
Woodland	Land dominated by trees or shrubs
Grassland	Grassland\Farmland
Residential	Land dominated with houses
Transport	Roads
River	Rappahannock and Rapidan river
Stream	Steams
Water	Water bodies, lakes
Impervious	Commercial and institutional area\mixed urban

150 years. Once all the images were geo-registered, we analyzed and classified the images into discrete land classes for all the data years. Our classification scheme consists of eight broad categories as tabulated in Table 2. This scheme was intended primarily for local use and was chosen especially for reconciling the contrasting natures of the 1867 and modern landscapes. Other detailed standard class schemes, such as NLCD, the National Gap Analysis, CLD, MODIS, and IGBP, are possible but not considered. Use of these detailed schemes will introduce unnecessary complications yet help less with our analysis. In this regard, our classification maps are not aimed to be directly comparable to the US NLCD data in terms of either spatial details or class categories.

To classify the old map or aerial images, we applied and tested three methods. First, we manually classified and digitized all the map and images via visual interpretation. This process was very laborious and in many cases, involved a tedious, frequent cross-checking in reference to high-quality images or geotagged photos available in Google Earth. This manual method provided the most accurate results. Therefore, we used these outputs as ground-truthing—with a nominal accuracy of 100%—for applying and testing the two automatic methods, as explained next. Second, one automatic method we chose is the pixel-based maximum likelihood classifier (MLC). Although new machine learning classifiers such as Random Forests (RF), Gaussian Processes, and SVM tend to be more powerful than MLC, they were not considered due to the enormous computation involved for classifying high-resolution images at pixel levels (Zhao et al., 2008).

As a third method, we applied an object-based classification approach through the combined use of the eCognition software and RF (Hultquist et al., 2014; Zhou et al., 2014). The images were first segmented into patches or objects. For each object, a total of 33 spectral or shape features were generated and used as inputs to RF, a machine learning algorithm that proved effective in many previous case studies (Hultquist et al., 2014). The grouping of pixels into objects can greatly reduce the computational costs for RF. A particularly attractive feature of RF is its capability of ranking the relative importance of inputs variables (Breiman, 2001), thereby allowing us to quantify the relative usefulness of shape and spectral features in the object-based classification for land-ocver discrimination.

Classification accuracies of the two automatic methods were assessed with regards to the manually-delineated classification maps for all the data years. In the comparison, we clumped the River, stream, and water bodies into a single water class, due to the significant spectral confusions among the three. Also, all the comparisons were made at a pixel-to-pixel basis, although the object-based method perform classification at the object level. A particular index we chose to quantify accuracy is the Kappa statistics:

$$\hat{K} = \frac{N \sum_{i=1}^{k} x_{ij} - \sum_{i=1}^{k} (x_{i+} \times x_{+j})}{N^2 - \sum_{i=1}^{k} (x_{i+} \times x_{+j})} \tag{1}$$

where N is the number of pixels, k is the number of rows in the matrix, x_{ij} is the number of observations in row i and column j, x_{i+} and x_{+j} are the marginal totals of row i and column j, respectively. More technical information about this statistic can be found in Congalton (1991).

2.4. Land-use history and changes in landscape metrics

We examined the new, long-term, high-resolution land maps derived above to characterize land-use change history for this region. Because our purpose here is to test the utility of our maps, the analysis in this part did not consider the two versions of maps from the automatic methods. Rather, we relied on the manually-derived land-cover maps, that is, the most accurate land-cover maps we obtained (Supplementary data in Appendix A). Foremost, we derived the overall change of the dominant land classes over time and quantified class-specific change using transition statistics. Also, landscape patterns are known to exert strong control on various landscape processes (Dalloz et al., 2017; Lausch et al., 2015; Yuan et al., 2015), be it ecological,

Table 3
Landscape metrics (McGarigal et al., 2002).

Class Metric	Description	Measurement
CA	Total (Class) Area equals the sum of the areas (m²) of all patches of the corresponding patch type, divided by 10,000 (to convert to hectares); that is, total class area.	$CA = \sum_{j=1}^{n} a_{ij} \left(\frac{1}{10,000} \right)$ a_{ij} = area (m²) of patch ij
NP	Number of Patches equals the number of patches of the corresponding patch type (class).	$NP = n_i$ n_i = number of patches of the same class i
LPI	Largest Patch Index equals the percentage of the landscape comprised by the largest patch.	$LPI = \frac{\max_{j=1}^{n}(a_{ij})}{A}(100)$ a_{ij} = area (m²) of patch ij. A = total landscape area (m²).
AREA-MN	Patch Area equals the area (m²) of the patch, divided by 10,000 (to convert to hectares).	$AREA = \sum_{j=1}^{n} a_{ij} \left(\frac{1}{10,000} \right)$ a_{ij} = area (m²) of patch ij
FRAC-MN	Fractal Dimension Index equals 2 times the logarithm of patch perimeter (m) divided by the logarithm of patch area (m²); the perimeter is adjusted to correct for the raster bias in perimeter.	$FRAC = \frac{2 \ln .25 P_{ij}}{\ln a_{ij}}$ p_{ij} = perimeter (m) of patch ij. a_{ij} = area (m²) of patch ij.
ENN-MN	Euclidean Nearest Neighbor Distance equals the distance (m) to the nearest neighboring patch of the same type, based on shortest edge-to-edge distance. Note that the edge-to-edge distances are from cell center to cell center.	$ENN = h_{ij}$ h_{ij} = distance (m) from patch ij to nearest neighboring patch of the same type (class), based on patch edge-to-edge distance, computed from cell center to cell center.
MN	MN (Mean) equals the sum, across all patches in the landscape, of the corresponding patch metric values, divided by the total number of patches. MN is given in the same units as the corresponding patch metric.	$MN = \frac{\sum_{i=1}^{m} \sum_{j=1}^{n} x_{ij}}{N}$

biophysical or biogeochemical. The standard way to quantify landscape patterns is to resort to landscape metrics, leveraging a suite of spatial statistics of patch configurations across the landscape. Landscape metrics in common use can be derived at the patch, class, or landscape level (McGarigal et al., 2002). The particular metrics we used and their acronyms are described in Table 3, including six class-based spatial metrics and a landscape-level metric. These metrics have been proven as useful predictors of many underlying ecological processes or good indicators of landscape quality.

3. Results and discussion

3.1. Land cover classification: the old map

The 1867 old map was geo-rectified in reference to the 2014 image reasonably well. The estimated registration error was 28.5 m based on a six-fold cross-validation of 31 pairs of ground control points. Our use of cross-validation rather than independent points is due to the difficulty in reliably pinpointing a large number of ground features common in both the 1867 and 2014 maps, a practical challenge also reported previously (Balletti, 2006; Cousins, 2001). The 31 pairs we chose include homesteads, historical markers, churches, road features, river features, farmhouses, fords, and other features believed to remain relatively stable. Even for these features, uncertainties could exist regarding their exact positions on the old map. Some features on the 1867 map were just symbolic representation rather than true physical boundaries; other features, such as the cross of a stream with a known road, would have been changed slightly (Fig. 2). Given the inaccuracies in pinpointing features, the error of 28.5 m may be an exaggeration of the true geometric error of the old map.

Despite the relatively large georegistration error compared to the resolutions of the aerial photos, the accuracy we obtained should be sufficient for land-cover analysis over a large landscape like ours (Chen et al., 2014; Lambin and Geist, 2008). Moreover, we found that most advanced automatic georeferencing functionalities were not helpful for registering this old map. In particular, with only a single band mono-color image, the map contains little to no spectral information for auto-

registration, a feature that is often leveraged to automatically match multiple digital multispectral images (Bentoutou et al., 2005; Shi and Jiang, 2016). Overall, the difficulties and issues encountered here are a generic problem faced in the processing of local historical maps. The solution lies more in local knowledge and familiarity with the area rather than computer techniques. To augment the utility of historical maps and reduce their locational errors, user-friendly tools may be developed to gather inputs from local citizens or experts. A successful example is David Rumsey's Historical Map Collection website; it provides an easy-to-use web GUI for any nonexpert viewers or users to contribute to the georeferencing and interpretation of historical maps or records (Goodchild, 2007; Rumsey and Williams, 2002).

Automatic classification of the historical map was found infeasible, regardless of the use of MLC at the pixel level or Random Forests (RF) at the object level. The difficulty arises from both the lack of spectral information and the idiosyncratic nature of the old map: Although the many land features are easily identifiable when interpreted visually, their symbolic representations are abstract and not amenable to image analysis algorithms. This is especially true due to the frequent lumping of multiple different types of features into a single layer (e.g., annotations over a farmhouse). The direct application of MLC to the raw pixels gave an overall classification accuracy of only 13.8%. This accuracy may be improved slightly if incorporating additional derived texture layers such as mean and skewness, giving an accuracy of 23.4%. Similarly, RF for object-based classification didn't yield any satisfactory classification. However, in the object-based analysis, the segmentation of the map resulted in some objects or patches that often characterize the boundaries of land parcels reasonably well (Fig. 3). Although this segmentation was fraught with numerous errors (e.g., those due to map annotation and symbols), the vector-based geometries of the resulting objects provided a useful starting point for manual editing and refinement. Overall, we found that automatic segmentation was the most useful computer-based analysis that aided in the processing of the historical map.
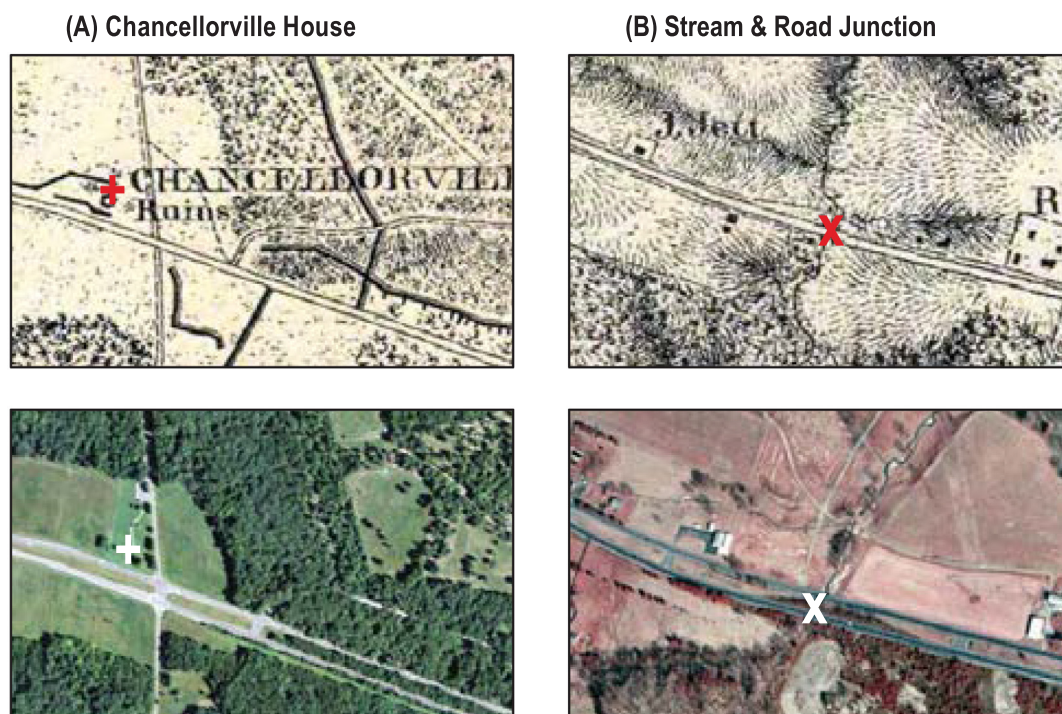
(A) Chancellorville House   (B) Stream & Road Junction

Fig. 2. Examples of the ground control points chosen to geo-rectify the 1867 old map: (a) Ruins of Chancerlorville House and (b) a road-stream crossing.

Small-scale Segmentation of the Old Map   **Large-Scale Segmentation of the Old Map**
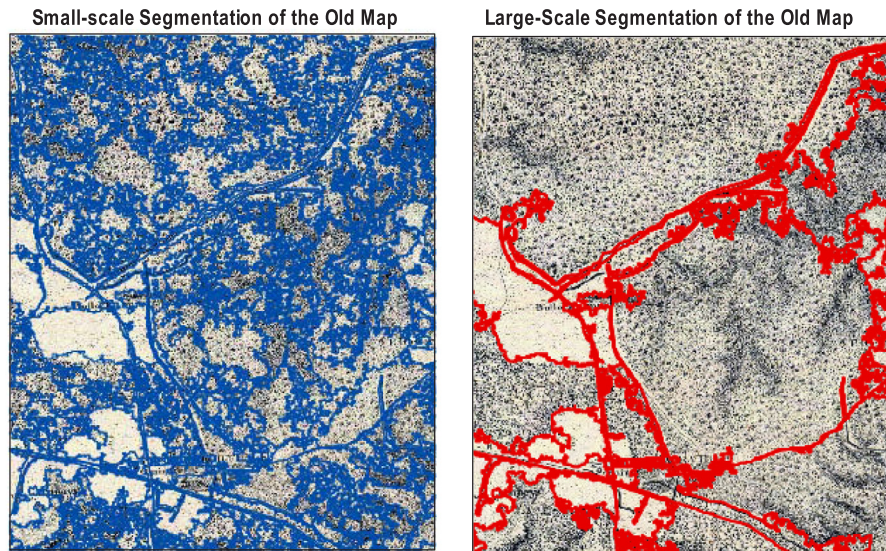

Fig. 3. Segmentation of the 1867 old map into objects at two contrasting spatial scales. Examples shown here demonstrate the potential utility of object-based image segmentation in aiding the analysis of historical maps.

3.2. Land cover classification: aerial photos

In contrast to the processing of the historical map, the analysis and classification of the aerial photos benefited considerably from digital image analysis, especially from the objected-based analysis. First of all, the 1981 aerial photo was accurately georegistered to the 2014 baseline image (RMSE = 2.52 m). More importantly, in classifying the aerial photo, the objected-based classifier based on RF outperformed the pixel-based MLC method. For ease of illustration, we use the 2014 image as an example: Fig. 4 depicts the comparisons of the three methods—visual interpretation, pixel-based MLC classification, and object-based RF classification. As explained earlier, the visual interpretation results were deemed as ground-truthing and used as reference data to assess the other two classifiers. The pixel-based classification with MLC shows a typical salt-and-pepper pattern, a well-known phenomenon that can often be suppressed through some additional spatial filters (Van de Voorde et al., 2007). This scattered pattern is particularly evident around residential areas. The overall pattern of the MLC-based classification therefore appears to deviate from the reference image derived from visual interpretation.

In contrast to the pixel-based classification, the object-based method resulted in a land-cover pattern that resembled the reference pattern more closely (Fig. 4), as a result of reduced spatial heterogeneity at the object levels (Im and Jensen, 2005). However, the object-based classification was found to depend strongly on the scale at which the

segmentation was performed—an effect that has been widely acknowledged and examined previously (Blaschke et al., 2004; Liu and Xia, 2010). We tested four different values for the scale parameters and found that the best classification accuracy of the four was 77.2% (Kappa statistics: 74.6%), obtained when the image was mostly over-segmented (i.e., small objects). This accuracy is better than the value of 75.4% (Kappa: 72.8%) obtained from the MLC pixel-based classifier. But when the image was under-segmented, the accuracy is only 68%, worse than the pixel-based classifier. Generally speaking, for a given image, there exists an optimal segmentation scale that has the least classification error (Liu and Xia, 2010). But no automatic procedures are available to pre-determine this optimum; instead, it needs to be pinpointed by trial-and-error, an exercise not pursued in this study.

Another important finding from our object-based classification concerns the relative usefulness of shape and geometry versus spectral features in classification (Fig. 5). The ranking of variable importance was made possible by a random permutation scheme in Random Forests. In our object-based classification, we incorporated a total of 33 object-level features (i.e., input variables for RF) and found that the top seven important features identified by RF were all spectral features, such as mean spectral values and standard deviation of spectral values (Fig. 5, top). The eighth most important variable is a geometry feature—the shape index (i.e., the border length of an image object divided by four times the square root of its area). Overall, our experiment suggests that the addition of object geometric features only improved
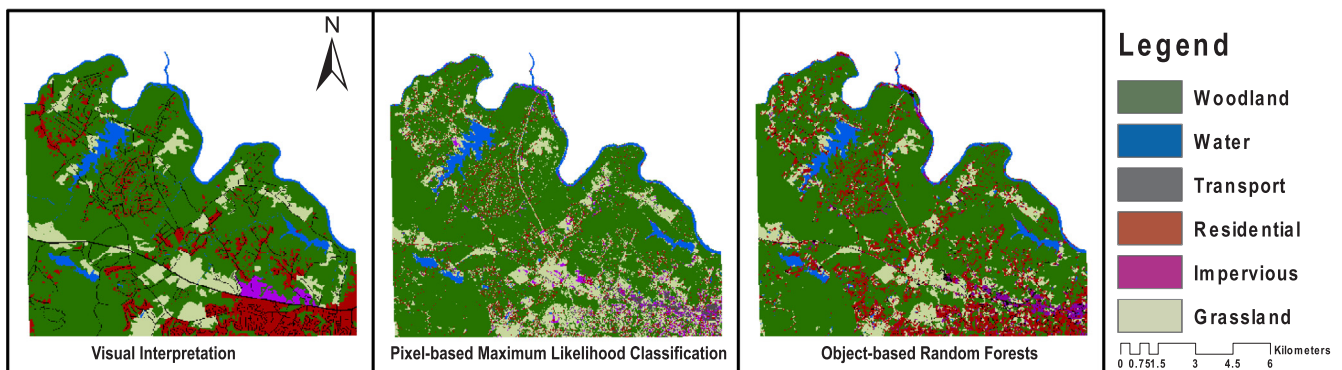

Fig. 4. Comparison of three classification methods based on the 2014 aerial photo—Visual interpretation (ground-truthing), Pixel-based Maximum Likelihood classification (MCL), and Object-based Random Forests.
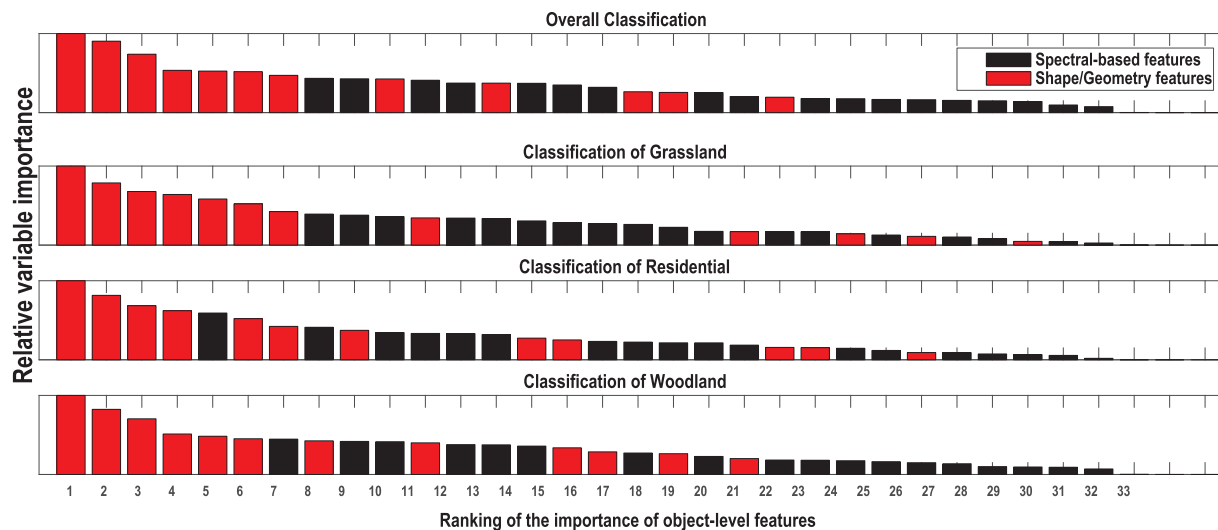
Fig. 5. In our object-based classification, shape/geometry features (black bars) were less useful or important than spectral-based features (red bars) for land-cover discrimination, as assessed and ranked by Random Forests. The top row is for the overall classification of all land-cover classes, and the bottom three rows for class-specific classification. (For interpretation of the references to color in this figure legend, the reader is referred to the web version of this article.)

the classification marginally. This finding is consistent with the above comparison result: The use of pixel-based spectral information alone gave an accuracy of 75.5%, as compared to 77.2% that resulted from the combined use of spectral and geometry/shape features accuracy.

Two caveats are noted about our object-based analyses. First, the exact ranking of variable/feature importance also depends on the land cover considered (Fig. 5). For example, the blue-band spectral value was found more important for classification of woodland than that of residential area. But still, the relative usefulness of geometric features was low for all classes, except that when classifying residential area, the object-level feature (i.e., a geometric feature) was the fifth most useful predictor. Second, the limited usefulness of shape/geometry features we found appeared to contradict the seeming belief we put in their value. To date, experimental evidence from other case studies that rigorously quantified the relative merits of spectral and shape features is still very limited. Regardless, decades of lessons learned on land cover classification indicate that the answers to questions about which method or variable is more useful tend to be case-specific and should be always interpreted in a relative sense (Foody, 2002).

3.3. Land use and land cover change

The five land-cover maps derived from visual interpretation captured the dramatic landscape changes from 1867 to 2014 (Fig. 6). (GIS shapefiles of the five digitized maps are available from Appendix A) During this 147-year period, 32.1% of the region changed in land cover. Settlement areas increased by 1, 850%. Woodland, grassland/cropland, and streams decreased in extent by 19%, 7%, and 18%, respectively. About 10.3% of the original woodland and 2.1% of the original grassland have been converted into residential areas. Despite the moderate loss of forest cover compared to other areas in the US, the landscape of the area, however, became more fragmented, especially due to expansion of transport networks: The extent of roads increased by 691%. These changes were largely driven by population growth and human activities. In roughly the same period, the population rose from 1, 356 to 129, 202 (Bureau, 2017), a 94 fold increase. Additional results about individual land-cover percentage and change statistics are summarized in Table 4. Spatial details about land change between 1869 and 2014 are presented in Fig. 7.

This region saw rapid urban development in recent decades, undergoing a gradual conversion from rural to suburban landscape (Table 4). The conversion and the influx of residents began during the

early 1960s, as a result of the construction of an interstate highway. But this early development falls within the years of data gap and was implicitly captured by the land change from 1860 to 1981, with a 1009% increase in settlement area. Accompanying the growing population is an increase water surface areas. In the 1867 map, no open water bodies (i.e., lakes and ponds) was present at all. In 2014, the coverage of open water bodies rose to approximately 2.71 km², attributed to the growing needs for clean water supply and the constructions of two reservoirs: Motts Run Reservoir built in 1991 and Hunting Run Reservoir. The extents and locations of both reservoirs were depicted in our maps (Figs. 6 & 7). In particular, Hunting Run Reservoir was impounded in 2002 and reached full pool in early 2009, a dynamic process revealed by the difference between the 2003 and 2014 land cover map (Fig. 6). Evident in the maps is also the addition and expansion of residential areas around Hunting Run Reservoir, especially at the southeastern flank.

We further demonstrated the utility of our maps by examining long-term changes in riverscape. The migrating channel of the Rappahannock River is evident. An overlaying of river boundaries between 1867 and 2014 highlights areas of the river that were subject to erosion and deposition (Fig. 8). This course migration is particularly conspicuous over and near the meandering parts of the river. Interpretation of the observed channel shift can be complicated due to various sources of uncertainties, such as georectification error and discrepancy in map dates pertaining to seasonality (Debnath et al., 2017; Glavan et al., 2013). But some of the observed changes in river morphology are unlikely to be caused by such uncertainties and should represent robust patterns, as supported by other lines of observational or theoretical evidence. For example, the channel width became narrower throughout the entire length, a pattern also evidenced in a visual comparison of real photos taken at Germanna Ford in 1864 and recently (Fig. 8). The wider channel in 1867 and the associated larger streamflow could be attributed largely to land-use practices of that time. Excessive runoff and erosion had been a well-documented issue after European settlement, depleting topsoil and deteriorating soil fertility. The woodland coverage in 1867 was larger than the current value, but the forests were a recovery from agricultural abandonment and due to poor soil fertility, they were mostly still low in stature. Therefore, surface runoff in 1867 is estimated to be larger, compared to the present. Overall, the changes in land-use altered the hydrological regime, thereby contributing to the observed patterns of erosion and deposition in the river and shifting the channel to a new equilibrium (Debnath
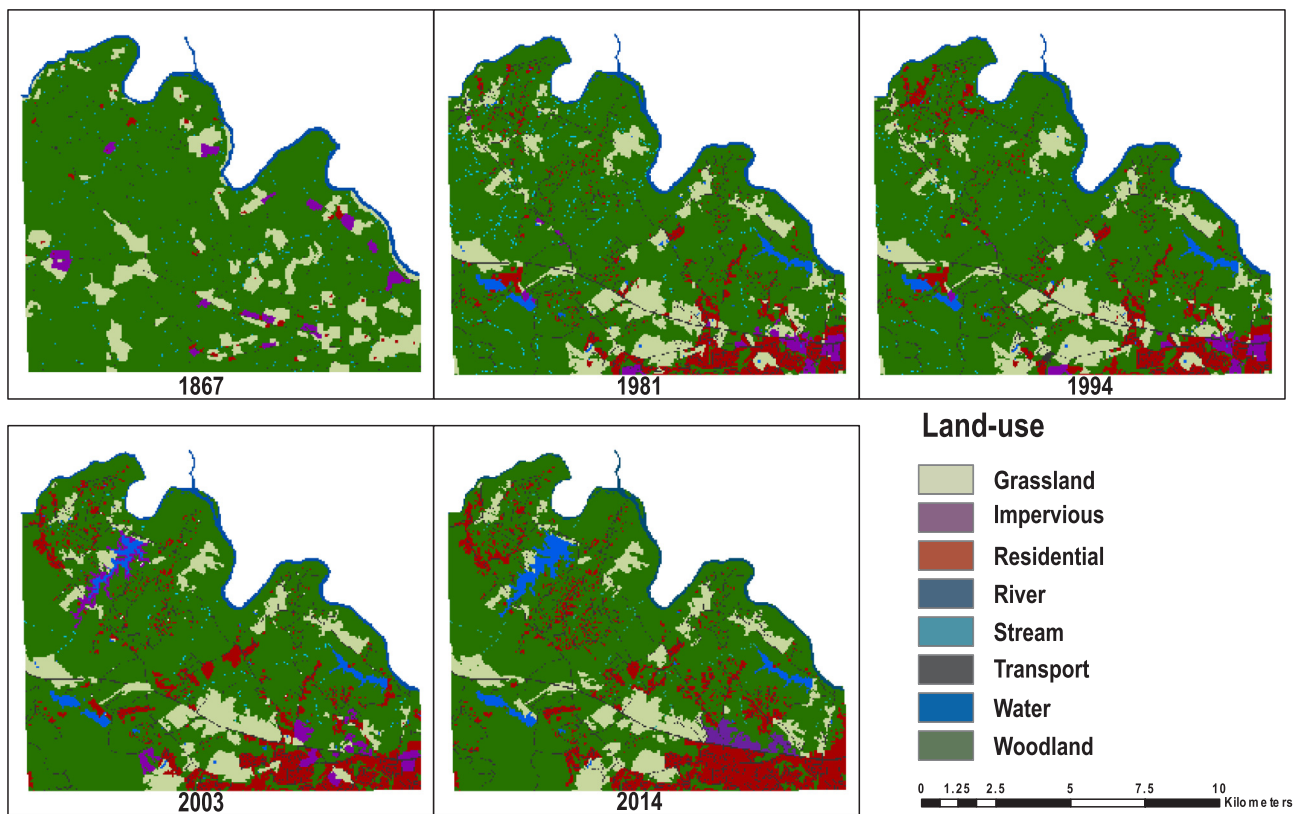
Fig. 6. Changes in land use/land cover from 1867 to 2014 captured at the five points in time. Results here are derived from visual interpretation (i.e., our first land classification method).

et al., 2017; Tagwireyi et al., 2017).

3.4. Landscape pattern analysis

Landscape metrics reveal systematic changes in spatial patterns of the landscape that cannot be characterized by overall changes in land-cover percentage alone. As examples, residential areas exhibited the largest growth rate in both class area (CA) and number of patches (NP). The significant increase in NP for residential area is consistent with the rapid population growth. In contrast, NP for the transport class decreased by −91.8%, although the transport class showed a high growth in total area. This pattern is due to the fact that the transport network becomes more connected with many linked neighboring patches. The largest patch index (LPI) and mean patch area (AREA_MN) of the transport class also increased, with a decreased mean fractal dimension index (FRAC_MN). FRAC_MN represents shape complexity: Larger values indicate more convoluted shapes (McGarigal et al., 2002). The re-arrangement of patches within the landscape is partially quantified by the mean Euclidean nearest neighbor distance (ENN_MN), that is, the

distance to the nearest neighboring patch of the same type based on shortest edge-to-edge distance. The ENN_MN values for patches of grassland, transport, and impervious surfaces decreased by 89.9%, 86.0%, and 96.1%, respectively, from the year 1867 to 2014. Other systematic shifts in landscape pattern are summarized in terms of various landscape metrics in Table 5. The values of these metrics as predictors of ecological or biophysical processes have been widely confirmed, but their such use requires building explanatory or predictive models, an exercise that will require detailed observations of the processes of interest.

As a caveat, when integrating historical and modern data, there generally exists a large temporal gap—more than 100 years in our case. Given the fortuitous nature of old maps, such gaps are almost inevitable (Axelsson and Östlund, 2001): The earlier an old map dates back, the larger the temporal gap may be. Whether or not a data gap will be problematic is case-specific. For our analyses, it is not because our purpose was to merely contrast the 1867 map with the modern images, but it becomes problematic for those applications on mapping landscapes continuously over time (Petit and Lambin, 2002b). Finding more

Table 4
Class areas and change statistics.

| Land cover types	1869	1981		1994		2003		2014		Overall Δ%
	km²	km²	Δ %	Km²	Δ %	Km²	Δ %	Km²	Δ %	
Woodland	89.019	76.428	−14.381	77.291	1.167	74.683	−3.375	72.930	−3.468	−19.097
Grassland	12.385	13.412	8.365	13.393	−0.306	11.491	−13.985	11.588	0.183	−6.826
Residential	0.656	7.284	1009.299	7.242	−0.659	10.528	45.402	12.803	21.695	1848.706
Transport	0.697	4.935	588.092	4.513	−9.037	4.439	−1.618	5.518	24.870	690.544
River	1.880	2.278	−16.755	2.213	0.000	2.071	−1.989	1.902	−8.160	−17.831
Stream	0.661	0.972	47.0500	0.792	−21.502	0.374	−63.889	0.273	−20.589	−58.886
Water	0.000	1.389	N/A	1.387	−0.288	1.888	36.193	2.706	43.326	N/A
Impervious	1.793	1.453	−18.907	1.310	−9.911	2.644	100.305	1.254	−52.610	−35.194
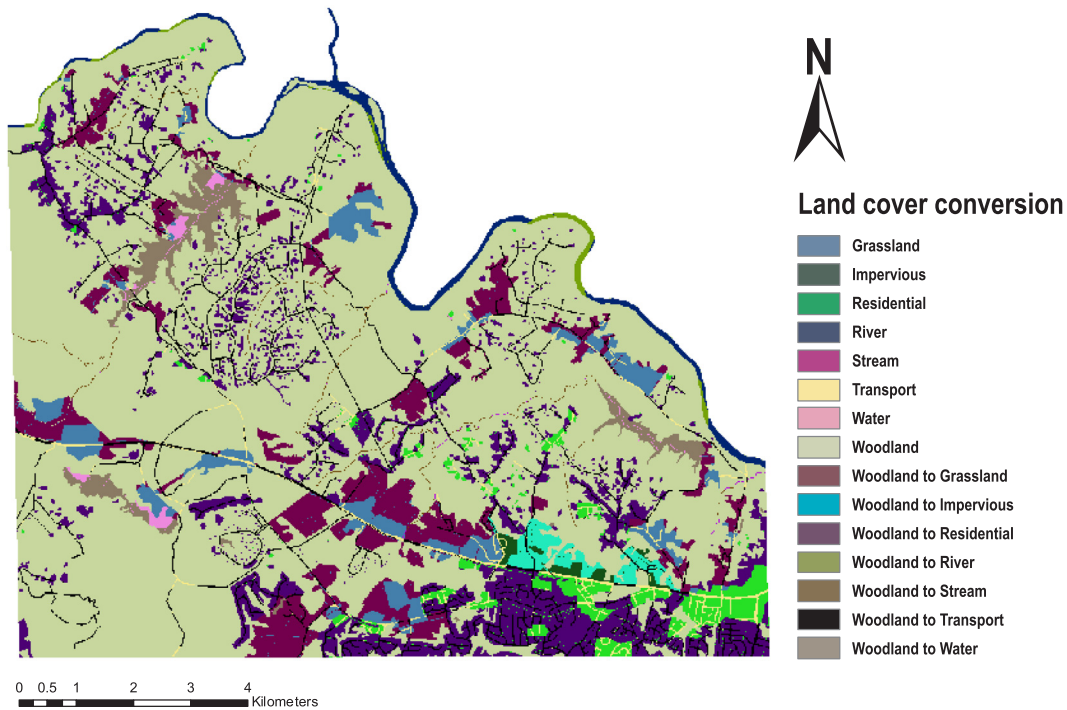
Fig. 7. Land cover transition from 1867 to 2014, as derived based on visual interpretation.

historical maps or images is not a solution because the problem is data scarcity itself. One viable, indirect solution is to estimate spatial landscape patterns for those data-gap years by using models or simulators, such as cellular automata, agent-based modeling, and statistical scaling (Groeneveld et al., 2017; Irwin and Geoghegan, 2001; Liu et al., 2017). Land-use simulators take existing maps as initial conditions and apply heuristic rules to model the change processes. Often enough, this gap-filling can be aided and constrained by incorporating other non-spatial historical data, such as deeds, sale records, and tax valuation (Goldewijk, 2001). Overall, a lesson learned is that we should strive to document and preserve our current data because they will become old data for future generations to explore—a voice also echoed in many other science communities (Griffin, 2017)

4. Conclusions

A lack of reliable, spatial-explicit historical land-use/land cover data remains a barrier to land change and global environmental change sciences. We demonstrated that this gap could be partially filled by resorting to historical maps. The integration of the civil war map and modern aerial photos helped to derive long-term land-use history and landscape change at high spatial resolutions from 1867 to 2014. The derived detailed pattern in land use change documented a conversion from rural to suburban landscape, offering valuable information to quantify ecological impacts and infer anthropogenic drivers of land changes. The value of our maps was also exemplified for tracking changes in river morphology. Our investigation is limited in spatial extent. But historical data similar to ours for other regions become increasingly available and accessible, for example, due to expiration of copyrights, improved data sharing technologies, and rising public
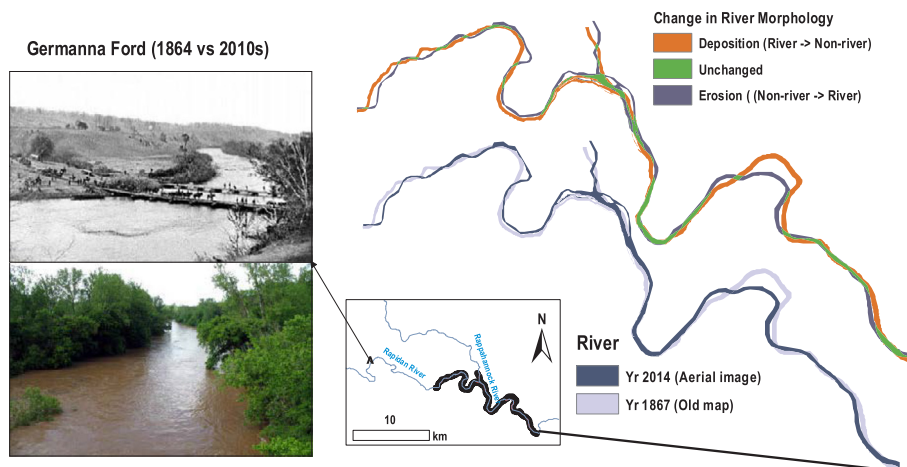

Fig. 8. Changes in Rappahannock River from 1867 to 2014. Photos taken at Germanna Ford in 1864 (left) and in 2010s (right) illustrate that streamflow was reduced, the river width was narrowed, and the riparian vegetation and riverine landscape were altered.

Table 5
Selected landscape metrics for 1869 and 2014 (meter).

Class	CA			NP			LPI		
	1869	2014	Δ %	1869	2014	Δ %	1869	2014	Δ %
Woodland	8945.937	7204.811	−19.46	812	1214	49.51	4.461	9.967	123.43
Grassland	1243.638	1150.593	−7.48	75	158	110.67	1.042	0.989	−5.09
Transport	69.693	551.609	691.48	49	4	−91.84	0.519	4.999	863.20
Residential	64.010	1280.143	1899.91	92	1150	1150.00	0.065	0.485	646.15
Impervious	193.560	125.356	−35.24	25	23	−8.00	0.178	0.699	292.70
River	274.586	199.499	−27.35	1	1	0.00	2.529	1.846	−27.01
Stream	66.263	27.281	−58.83	187	27	−85.56	0.048	0.035	−27.08
Class	AREA-MN			FRAC-MN			ENN-MN		
	1869	2014	Δ %	1869	2014	Δ %	1869	2014	Δ %
Woodland	11.017	5.935	−46.13	1.116	1.218	9.14	4.146	7.130	71.97
Grassland	1.422	7.282	412.10	1.085	1.181	8.85	186.781	18.848	−89.91
Transport	1.422	137.902	9597.75	1.413	1.279	−9.48	86.627	107.044	23.57
Residential	0.696	1.113	59.91	1.252	1.119	−10.62	289.787	40.557	−86.00
Impervious	7.742	5.450	−29.60	1.112	1.167	4.95	334.745	13.106	−96.08
River	274.586	199.499	−27.35	1.331	1.350	1.43	N/A	N/A	N/A
Stream	0.354	1.010	185.31	1.638	1.010	−38.34	62.094	89.759	44.55

interest. These old data are still under-utilized. We hope that the empirical evidence reported here provides an impetus for further research on leveraging the value and power of such historical data or maps to advance land-use sciences.

Methodologically speaking, the use of historical maps can involve tedious manual processing. The information extraction process may be expedited by computer image analysis, but the achieved level of automation will be case-specific. Automatic classification of our historical map was difficult, if not impossible, regardless of the use of pixel-based or object-based classifiers. However, object-based analysis proved useful in meaningfully segmenting the old map and facilitating the map digitization. When tested upon modern aerial imagery, object-based classification performed better than the pixel-based method but required fine-tuning for image segmentation. Our variable importance analysis via Random Forests suggests that most of the geometry/shape features were useless or only marginally useful for object-level classification. The generality of these findings needs to be further tested in more case studies, especially regarding the effective use of machine learning to assist in object-based classification. Irrespective of which techniques are used, a lesson learned is that the integration of historical data and digital remote sensing imagery would be difficult or impossible without metadata or other ancillary information. Old maps, for example, become less useful if not georeferenced reliably. Likewise, the vast majority of data that we are collecting or generating now, such as maps, paintings, digital photos, videos, and citizen science data, may serve as baseline data for future generations. Our preserving and geotagging such data will do our future counterparts a service in documenting future landscape changes.

Acknowledgements

Appendix A. Supplementary data

Supplementary data associated with this article can be found, in the online version, at https://doi.org/10.1016/j.ecolind.2018.08.004.

References

Arnett, J.T., Coops, N.C., Daniels, L.D., Falls, R.W., 2015. Detecting forest damage after a low-severity fire using remote sensing at multiple scales. Int. J. Appl. Earth Obs. Geoinf. 35, 239–246.
Axelsson, A.-L., Östlund, L., 2001. Retrospective gap analysis in a Swedish boreal forest landscape using historical data. For. Ecol. Manage. 147, 109–122.
Balletti, C., 2006. Georeference in the analysis of the geometric content of early maps. e-Perimetron 1, 32–42.
Belgiu, M., Drăguţ, L., 2016. Random forest in remote sensing: a review of applications and future directions. ISPRS J. Photogramm. Remote Sens. 114, 24–31.
Bentoutou, Y., Taleb, N., Kpalma, K., Ronsin, J., 2005. An automatic image registration for applications in remote sensing. IEEE Trans. Geosci. Remote Sens. 43, 2127–2137.
Bicík, I., Kupková, L., Jeleček, L., Kabrda, J., Štych, P., Janoušek, Z., Winklerová, J., 2015. Land Use Changes in Czechia 1845–2010. In: Land Use Changes in the Czech Republic 1845–2010. Springer, pp. 95–170.
Blaschke, T., 2010. Object based image analysis for remote sensing. ISPRS J. Photogramm. Remote Sens. 65, 2–16.
Blaschke, T., Burnett, C., Pekkarinen, A., 2004. Image segmentation methods for object-based analysis and classification. In: Remote Sensing Image Analysis: Including the Spatial Domain. Springer, pp. 211–236.
Breiman, L., 2001. Random forests. Mach. Learn. 45, 5–32.
Bright, R.M., Davin, E., O'Halloran, T., Pongratz, J., Zhao, K., Cescatti, A., 2017. Local temperature response to land cover and management change driven by non-radiative processes. Nat. Clim. Change 7, 296–302.
Bureau, U.S.C., 2017. US Population Data, Retrieved from < https://ask.census.gov/prweb/PRServletCustom/YACFBFye-rFIz_FoGtyvDRUGg1Uzu5Mn*/!STANDARD?pyActivity=pyMobileSnapStart&ArticleID=KCP-3282 > .
Chen, G., Hay, G.J., Carvalho, L.M., Wulder, M.A., 2012. Object-based change detection. Int. J. Remote Sens. 33, 4434–4457.
Chen, G., Zhao, K., Powers, R., 2014. Assessment of the image misregistration effects on object-based change detection. ISPRS J. Photogramm. Remote Sens. 87, 19–27.
Chen, G., Powers, R.P., de Carvalho, L.M., Mora, B., 2015. Spatiotemporal patterns of tropical deforestation and forest degradation in response to the operation of the Tucuruí hydroelectric dam in the Amazon basin. Appl. Geogr. 63, 1–8.
Congalton, R.G., 1991. A review of assessing the accuracy of classifications of remotely sensed data. Remote Sens. Environ. 37, 35–46.
Congalton, R.G., Gu, J., Yadav, K., Thenkabail, P., Ozdogan, M., 2014. Global land cover mapping: a review and uncertainty analysis. Remote Sens. 6, 12070–12093.
Cousins, S.A., 2001. Analysis of land-cover transitions based on 17th and 18th century cadastral maps and aerial photographs. Landscape Ecol. 16, 41–54.
Dalloz, M.F., Crouzeilles, R., Almeida-Gomes, M., Papi, B., Prevedello, J.A., 2017. Incorporating landscape ecology metrics into environmental impact assessment in the Brazilian Atlantic Forest. Perspect. Ecol. Conserv.
Debnath, J., Pan, N.D., Ahmed, I., Bhowmik, M., 2017. Channel migration and its impact on land use/land cover using RS and GIS: a study on Khowai River of Tripura, North-East India. Egypt. J. Remote Sens. Space Sci.
Foley, J.A., DeFries, R., Asner, G.P., Barford, C., Bonan, G., Carpenter, S.R., Chapin, F.S., Coe, M.T., Daily, G.C., Gibbs, H.K., 2005. Global consequences of land use. Science 309, 570–574.
Foody, G.M., 2002. Status of land cover classification accuracy assessment. Remote Sens. Environ. 80, 185–201.
Foster, D.R., 1992. Land-use history (1730–1990) and vegetation dynamics in central

New England, USA. J. Ecol. 753–771.

Fuchs, R., Verburg, P.H., Clevers, J.G., Herold, M., 2015. The potential of old maps and encyclopaedias for reconstructing historic European land cover/use change. Appl. Geogr. 59, 43–55.

Gitas, I.Z., San-Miguel-Ayanz, J., Chuvieco, E., Camia, A., 2014. Advances in remote sensing and GIS applications in support of forest fire management. Int. J. Wildland Fire 23, 603–605.

Glavan, M., Pintar, M., Volk, M., 2013. Land use change in a 200-year period and its effect on blue and green water flow in two Slovenian Mediterranean catchments—lessons for the future. Hydrol. Process. 27, 3964–3980.

Goldewijk, K.K., 2001. Estimating global land use change over the past 300 years: the HYDE database. Global Biogeochem. Cycles 15, 417–433.

Goodchild, M.F., 2007. Citizens as sensors: the world of volunteered geography. GeoJournal 69, 211–221.

Griffin, E., 2017. Rescue old data before it's too late. Nature 545.

Groeneveld, J., Müller, B., Buchmann, C.M., Dressler, G., Guo, C., Hase, N., Hoffmann, F., John, F., Klassert, C., Lauf, T., 2017. Theoretical foundations of human decision-making in agent-based land use models–a review. Environ. Modell. Software 87, 39–48.

Haase, D., Walz, U., Neubert, M., Rosenberg, M., 2007. Changes to Central European landscapes—analysing historical maps to approach current environmental issues, examples from Saxony, Central Germany. Land Use Policy 24, 248–263.

Hansen, M.C., Potapov, P.V., Moore, R., Hancher, M., Turubanova, S., Tyukavina, A., Thau, D., Stehman, S., Goetz, S., Loveland, T., 2013. High-resolution global maps of 21st-century forest cover change. Science 342, 850–853.

Hultquist, C., Chen, G., Zhao, K., 2014. A comparison of Gaussian process regression, random forests and support vector regression for burn severity assessment in diseased forests. Remote Sens. Lett. 5, 723–732.

Hussain, M., Chen, D., Cheng, A., Wei, H., Stanley, D., 2013. Change detection from remotely sensed images: from pixel-based to object-based approaches. ISPRS J. Photogramm. Remote Sens. 80, 91–106.

Im, J., Jensen, J.R., 2005. A change detection model based on neighborhood correlation image analysis and decision tree classification. Remote Sens. Environ. 99, 326–340.

Irwin, E.G., Geoghegan, J., 2001. Theory, data, methods: developing spatially explicit economic models of land use change. Agric. Ecosyst. Environ. 85, 7–24.

Jensen, J.R., 2009. Remote Sensing of the Environment: An Earth Resource Perspective 2/ e. Pearson Education India.

Johnson, K.M., Ouimet, W.B., 2016. Physical properties and spatial controls of stone walls in the northeastern USA: implications for Anthropocene studies of 17th to early 20th century agriculture. Anthropocene 15, 22–36.

Joshi, N., Baumann, M., Ehammer, A., Fensholt, R., Grogan, K., Hostert, P., Jepsen, M.R., Kuemmerle, T., Meyfroidt, P., Mitchard, E.T., 2016. A review of the application of optical and radar remote sensing data fusion to land use mapping and monitoring. Remote Sens. 8, 70.

Killeen, T., Guerra, A., Calzada, M., Correa, L., Calderon, V., Soria, L., Quezada, B., Steininger, M., 2008. Total historical land-use change in eastern Bolivia: who, where, when, and how much? Ecol. Soc. 13.

Lambin, E.F., Geist, H.J., 2008. Land-Use and land-cover Change: Local Processes and Global Impacts. Springer Science & Business Media.

Lausch, A., Blaschke, T., Haase, D., Herzog, F., Syrbe, R.-U., Tischendorf, L., Walz, U., 2015. Understanding and quantifying landscape structure–a review on relevant process characteristics, data models and landscape metrics. Ecol. Model. 295, 31–41.

Li, W., Fu, H., Yu, L., Gong, P., Feng, D., Li, C., Clinton, N., 2016. Stacked Autoencoder-based deep learning for remote-sensing image classification: a case study of African land-cover mapping. Int. J. Remote Sens. 37, 5632–5646.

Liu, Y., Hu, Y., Long, S., Liu, L., Liu, X., 2017. Analysis of the effectiveness of urban land-use-change models based on the measurement of spatio-temporal, dynamic urban growth: A cellular automata case study. Sustainability 9, 796.

Liu, D., Xia, F., 2010. Assessing object-based classification: advantages and limitations. Remote Sens. Lett. 1, 187–194.

Loran, C., Munteanu, C., Verburg, P.H., Schmatz, D.R., Bürgi, M., Zimmermann, N.E., 2017. Long-term change in drivers of forest cover expansion: an analysis for Switzerland (1850–2000). Reg. Environ. Change 1–13.

Mahowald, N.M., Randerson, J.T., Lindsay, K., Munoz, E., Doney, S.C., Lawrence, P., Schlunegger, S., Ward, D.S., Lawrence, D., Hoffman, F.M., 2017. Interactions between land use change and carbon cycle feedbacks. Global Biogeochem. Cycles 31, 96–113.

Mansfield, J.R., 1977. A History of Early Spotsylvania. Virginia Book Company.

McGarigal, K., Cushman, S.A., Neel, M.C., Ene, E., 2002. FRAGSTATS: spatial pattern analysis program for categorical maps.

Newbold, T., Hudson, L.N., Hill, S.L., Contu, S., Lysenko, I., Senior, R.A., Börger, L., Bennett, D.J., Choimes, A., Collen, B., 2015. Global effects of land use on local terrestrial biodiversity. Nature 520, 45–50.

Olah, B., 2009. Historical maps and their application in landscape ecological research. Ekológia 28, 143.

Orwig, D.A., Abrams, M.D., 1994. Land-use history (1720–1992), composition, and dynamics of oak–pine forests within the Piedmont and Coastal Plain of northern Virginia. Can. J. For. Res. 24, 1216–1225.

Ostafin, K., Iwanowski, M., Kozak, J., Cacko, A., Gimmi, U., Kaim, D., Psomas, A., Ginzler, C., Ostapowicz, K., 2017. Forest cover mask from historical topographic maps based on image processing. Geosci. Data J. 4, 29–39.

Pavelková, R., Frajer, J., Havlíček, M., Netopil, P., Rozkošný, M., David, V., Dzuráková, M., Šarapatka, B., 2016. Historical ponds of the Czech Republic: an example of the interpretation of historic maps. J. Maps 12, 551–559.

Petit, C., Lambin, E., 2002a. Impact of data integration technique on historical land-use/ land-cover change: comparing historical maps with remote sensing data in the Belgian Ardennes. Landscape Ecol. 17, 117–132.

Petit, C., Lambin, E., 2002b. Long-term land-cover changes in the Belgian Ardennes (1775–1929): model-based reconstruction vs. historical maps. Glob. Change Biol. 8, 616–630.

Prestele, R., Arneth, A., Bondeau, A., Noblet-Ducoudré, N.D., Pugh, T.A., Sitch, S., Stehfest, E., Verburg, P.H., 2017. Current challenges of implementing anthropogenic land-use and land-cover change in models contributing to climate change assessments. Earth Syst. Dyn. 8, 369–386.

Pu, R., Landry, S., 2012. A comparative analysis of high spatial resolution IKONOS and WorldView-2 imagery for mapping urban tree species. Remote Sens. Environ. 124, 516–533.

Rumsey, D., Williams, M., 2002. Historical maps in GIS. na.

Schaffer, G., Levin, N., 2016. Reconstructing nineteenth century landscapes from historical maps—the Survey of Western Palestine as a case study. Landscape Res. 41, 360–379.

Shalaby, A., Tateishi, R., 2007. Remote sensing and GIS for mapping and monitoring land cover and land-use changes in the Northwestern coastal zone of Egypt. Appl. Geogr. 27, 28–41.

Shi, X., Jiang, J., 2016. Automatic registration method for optical remote sensing images with large background variations using line segments. Remote Sens. 8, 426.

Srinath, I., Millington, A.C., 2016. Evaluating the potential of the original texas land survey for mapping historical land and vegetation cover. Land 5, 4.

Tagwireyi, P., Sullivan, S.M.P., Zhao, K., 2017. Associations between riverine landscape patches and internal and external environmental determinants are scale dependent: evidence from the Scioto River, USA. Fundam. Appl. Limnol. 235–249.

Van de Voorde, T., De Genst, W., Canters, F., 2007. Improving pixel-based VHR land-cover classifications of urban areas with post-classification techniques. Photogramm. Eng. Remote Sens. 73, 1017.

Walter, V., 2004. Object-based classification of remote sensing data for change detection. ISPRS J. Photogramm. Remote Sens. 58, 225–238.

Wu, J., 2013. Landscape sustainability science: ecosystem services and human well-being in changing landscapes. Landscape Ecol. 28, 999–1023.

Xiao, J., Shen, Y., Ge, J., Tateishi, R., Tang, C., Liang, Y., Huang, Z., 2006. Evaluating urban expansion and land use change in Shijiazhuang, China, by using GIS and remote sensing. Landscape Urban Plann. 75, 69–80.

Yuan, J., Cohen, M.J., Kaplan, D.A., Acharya, S., Larsen, L.G., Nungesser, M.K., 2015. Linking metrics of landscape pattern to hydrological process in a lotic wetland. Landscape Ecol. 30, 1893–1912.

Zhao, K., García, M., Liu, S., Guo, Q., Chen, G., Zhang, X., Zhou, Y., Meng, X., 2015. Terrestrial lidar remote sensing of forests: Maximum likelihood estimates of canopy profile, leaf area index, and leaf angle distribution. Agric. For. Meteorol. 209, 100–113.

Zhao, K., Jackson, R.B., 2014. Biophysical forcings of land-use changes from potential forestry activities in North America. Ecol. Monogr. 84, 329–353.

Zhao, K., Popescu, S., Zhang, X., 2008. Bayesian learning with Gaussian processes for supervised classification of hyperspectral data. Photogramm. Eng. Remote Sens. 74, 1223–1234.

Zhao, K., Popescu, S., Meng, X., Pang, Y., Agca, M., 2011. Characterizing forest canopy structure with lidar composite metrics and machine learning. Remote Sens. Environ. 115, 1978–1996.

Zhao, K., Suarez, J.C., Garcia, M., Hu, T., Wang, C., Londo, A., 2018. Utility of multi-temporal lidar for forest and carbon monitoring: Tree growth, biomass dynamics, and carbon flux. Remote Sens. Environ. 204, 883–897.

Zhou, W., Cadenasso, M.L., Schwarz, K., Pickett, S.T., 2014. Quantifying spatial heterogeneity in urban landscapes: integrating visual interpretation and object-based classification. Remote Sens. 6, 3369–3386.

Zhou, Y., Smith, S.J., Zhao, K., Imhoff, M., Thomson, A., Bond-Lamberty, B., Asrar, G.R., Zhang, X., He, C., Elvidge, C.D., 2015. A global map of urban extent from nightlights. Environ. Res. Lett. 10, 054011.